Nanoscale

PAPER

View Article Online
View Journal | View Issue

Cite this: *Nanoscale*, 2019, **11**, 1236

In situ manipulation of fluorescence resonance energy transfer between quantum dots and monolayer graphene oxide by laser irradiation†

Wenjun He,[a,b] Chengbing Qin, *[a,b] Zhixing Qiao,[a,b] Yani Gong,[a,b] Xiaorong Zhang,[a,b] Guofeng Zhang,[a,b] Ruiyun Chen,[a,b] Yan Gao,[a,b] Liantuan Xiao*[a,b] and Suotang Jia[a,b]

The unique optical properties of solution-processable colloidal semiconductor quantum dots (QDs) highlight their promising applications in the next generation of optoelectronic and biomedical technologies. In order to optimize these applications, the tunability of QDs' optical properties is always highly desired. Although the tuning during synthesis stages has been intensively investigated, the *in situ* alteration after device fabrication is still limited. Here we report the tuning of the optical properties of CdSeTe/ZnS QDs through an *in situ* manipulation of fluorescence resonance energy transfer (FRET) between QDs and monolayer graphene oxide (GO). By increasing the acceptor's absorption ability of GO through laser irradiation, the efficiency of FRET between QDs and GO has been substantially improved from 29.7% to 70.0%. The corresponding energy transfer rate is enhanced by 5.5 times. These results can be well explored by a spectral overlap between the fluorescence emission of QDs and the absorption of original or reduced GO. Our scheme, with the features of *in situ* manipulation, high spatial resolution and wireless steering, enables the potential functionality of such hybrid structures in optoelectronic applications.

Received 27th September 2018,
Accepted 6th December 2018

DOI: 10.1039/c8nr07858k

rsc.li/nanoscale

1. Introduction

Zero-dimensional (0D) quantum dots (QDs) or colloidal semiconductor nanocrystals have been the focus of intensive investigation over the past several decades, in view of their unique optical properties including high brightness, photochemical stability, and wide excitation but narrow emission bands. The power of these advantages has motivated increasingly active research studies aimed at applying QDs into the next generation of optoelectronic devices,[1–3] such as solar cells,[4] photodetectors,[5] field-effect transistors,[6] single photon sources,[7] and light-emitting devices.[8] In order to fabricate and optimize these devices, the tunability of the optical properties of QDs is always highly desired. So far, many wonderful research studies have been focused on the tuning of the optical properties of QDs during their synthesis stages by changing their size,[9] shape,[10] doping,[11] alloying,[12] and band gap offsets of the core–shell.[13] On the other hand, these properties can also be modified by utilizing the interaction between QDs and substrates or coverings during device fabrication. Among them, two-dimensional (2D) materials have been most strikingly highlighted recently, due to the strong interaction in these 0D–2D hybrid structures and their tunability as a function of 2D materials' layer thickness.[14–16]

2D atomically thin materials, including graphene and its derivatives,[17] as well as transition metal dichalcogenides (such as MoS_2, WSe_2)[18] show strong layer-dependent properties and applications. By changing the layer thickness, the interactions in the 0D–2D hybrid structures (including fluorescence resonance energy transfer (FRET) or nonradiative energy transfer (NRET) as well as charge transfer) can be well modified. Thus, the tuning of the optical properties of QDs can be achieved. In 2010, Brus' group reported that the rate of energy transfer from CdSe/ZnS QDs to graphene increased significantly with the number of graphene layers,[19] which has also been proven by Zang and coworkers in the CdSe/ZnS–SnS_2 hybrid structure.[14] However, in contrast, Raja and Prins reported increased rates with a decreasing number of MoS_2 layers,[16,20] where the highest fluorescence quenching (>95%) was observed for monolayer MoS_2. The opposite trends with the thickness of 2D materials have been attributed to the com-

[a]*State Key Laboratory of Quantum Optics and Quantum Optics Devices, Institute of Laser Spectroscopy, Shanxi University, Taiyuan, 030006, China.*
E-mail: chbqin@sxu.edu.cn, xlt@sxu.edu.cn; Fax: +86-0351-7113-863; Tel: +86-0351-7113-805
[b]*Collaborative Innovation Center of Extreme Optics, Shanxi University, Taiyuan, Shanxi, 030006, China*

†Electronic supplementary information (ESI) available. See DOI: 10.1039/c8nr07858k

petition between the absorption and screening of the local electric field.[16,20] Furthermore, the rate of energy transfer from individual QDs to 2D materials has been determined to be proportional to r^{-4}, where r is the distance between QDs and 2D materials.[21] This suggests that the energy transfer in 0D–2D hybrid structures is more efficient than that in 0D–0D structures, which is proportional to r^{-6}.[22] In these reports, the fluorescence intensity and lifetime of QDs have been substantially tuned by utilizing different 2D materials and/or different thicknesses during device fabrication. However, the *in situ* manipulation of QDs' properties after device fabrication or during the synthesis stages, according to the demand in practical applications, is still limited.

In this work, we present an *in situ* manipulation of the optical properties of CdSeTe/ZnS core–shell QDs after device fabrication. This scheme is achieved by altering the efficiency and rate of FRET from QDs to monolayer graphene oxide (GO). According to the classical theory, the efficiency and rate of FRET depend on the degree of spectral overlap between the donor emission and the acceptor absorption,[22] therefore we enhance the absorption of monolayer GO by *in situ* reduction through laser irradiation, and thus realize the manipulation of FRET. The fluorescence intensity and lifetime of individual QDs on glass (regarded as non-interaction with surroundings), GO and reduced GO (RGO) with different irradiation durations have been measured. The probability distributions of photoblinking events for individual QDs have also been analyzed to exclude the charge transfer during this process. Lastly, the efficiency is increased from 29.7% of QDs on GO to 70.0% of those on RGO with the longest irradiation duration. The corresponding rate is improved from 0.251×10^7 s^{-1} to 1.386×10^7 s^{-1}. Our scheme, with the features of *in situ* manipulation, high spatial resolution and wireless steering, will provide a new approach for tuning FRET between QDs and GO, and thus tune the optical properties of QDs as needed.

2. Results and discussion

Fig. 1a presents the hybrid QD–GO structure with a cross-sectional view. Here the near-infrared emitting (NIR) CdSeTe/ZnS core–shell QDs were selected, in view of their promising applications in medical labeling and solar cells,[23,24] as well as their intensive fluorescence emission overlapping with the optical absorption of GO, which enables strong interaction between QDs and GO. Detailed information about sample preparation can be found in Methods. Briefly, the GO dispersion was spin-coated on a cleaned glass coverslip initially. According to the

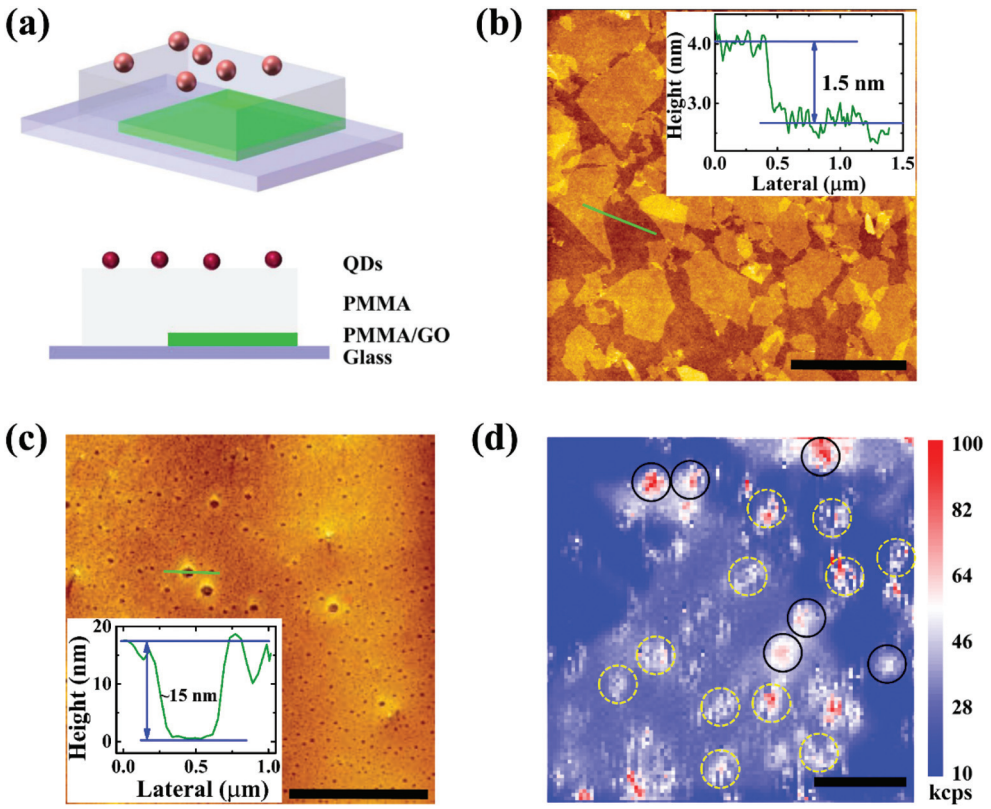

Fig. 1 (a) Schematic representation of the QD–GO hybrid structure. (b, c) Atomic force microscopy of the prepared GO film and the PMMA film. The insets are the height profiles of selected lines. Scale bar: 2 μm. (d) Fluorescence intensity imaging of the QD–GO hybrid structure. The dashed circles represent the fluorescence from individual QDs, and the solid circles represent the fluorescence from aggregated QDs, respectively. Scale bar: 2 μm.

characterization of atomic force microscopy (AFM) presented in Fig. 1b, the thickness of most films is about 1.5 nm, indicating that the prepared GO films are monolayer.[25,26] Generally, previous 0D–2D hybrid structures were prepared by loading QDs atop 2D materials directly,[14,20,27] and then their optical properties and modifications were investigated. However, it is found that when the CdSeTe/ZnS QDs were directly loaded on the top of the GO surface, their fluorescence was almost fully quenched. This phenomenon is consistent with previous studies in aqueous environments,[28,29] resulting from the strong interaction between QDs and GO. To hold the interaction strength in a favorable region, the transparent insulating polymer, poly(methyl methacrylate) (PMMA), was fabricated on the top of the GO surface firstly, and then QDs were loaded atop the PMMA film, as illustrated in Fig. 1a. To extend the tunability of the interaction between QDs and GO, the thickness of the PMMA film has been carefully optimized to be 15 nm. The presence of the PMMA film has been checked using a cross-sectional scanning electron microscope (SEM) (detailed information for the thickness of the PMMA film has been supplied in the ESI, as shown in Fig. S1†), and the corresponding thickness has been confirmed by AFM,[30] as shown in Fig. 1c. The size and height of QDs have also been characterized using a transmission electron microscope (TEM) and AFM, as shown in Fig. S2,† with the sizes varying from 3.6 nm to 9.6 nm. The wide distribution in size suggests the strong anisotropic properties of QDs.

Fig. 1d shows a confocal fluorescence imaging of GO loading with QDs. A large flake with a fluorescence intensity of about 45 thousand counts per second (kcps) can be distinctly observed in the fluorescence imaging. Undoubtedly, this flake originates from the fluorescence emission of monolayer GO, which has also been confirmed by Raman spectroscopy, as shown in Fig. S3.† On and beyond monolayer GO, some discrete patterns with stronger fluorescence intensity can be visualized, as the dashed circles highlighted in Fig. 1d. The discreteness mainly arises from the photoblinking of QDs during fluorescence imaging, confirming that these patterns originate from the fluorescence emission of individual QDs (the areas marked with solid circles with less discreteness represent the fluorescence from aggregated QDs. The method of determining individual QDs has been supplied and discussed in the ESI, as shown in Fig. S4 and S5†). From Fig. 1d, we can generally conclude that the fluorescence intensity of individual QDs on the top of monolayer GO is weaker than that beyond GO, suggesting the strong interaction between QDs and GO. Compared with the QDs on the top of GO (with PMMA between them, as shown in Fig. 1a), the QDs beyond GO can be treated as those on the top of the glass coverslip, which can be regarded as the case of non-interaction. This hypothesis has been proved by the similar fluorescence lifetime of QDs on glass, on PMMA and in toluene, as shown in Fig. S6.† Thus, the QDs on the PMMA will be used as a control experiment to reveal the interaction between QDs and GO. For the sake of simplicity, if not specially mentioned, the QDs on the top of and beyond monolayer GO are named "on GO" and "on glass" hereinafter for short, respectively.

To *in situ* manipulate and investigate the interaction between QDs and GO, a 485 nm laser with both continuous wave (CW) and pulsed wave modes was used in the experiment. The CW mode was used as the control laser to irradiate and reduce GO with a power of 1 mW, while the pulsed mode was used as the probe laser to collect the fluorescence emission from QDs with an average power of 10 μW and a repetition of 1 MHz. Considering that the power of the probe laser is two orders of magnitude lower than the control laser, the reduction effect on the GO film during fluorescence probing can be ignored. Furthermore, the optical properties of the QDs themselves show no significant change before and after CW laser irradiation especially for QDs' lifetime, as illustrated in Fig. S7 and S8.† Fig. 2a presents the fluorescence trajectory of individual QDs varied as a function of the irradiation duration of the control laser. Note that the fluorescence exhibits a strong background at the beginning. With the increase of laser irradiation, the background rapidly quenches to a weak and stable intensity. As we reported in the previous studies,[31] this background originates from the fluorescence emission of GO, the quenching effect is a result of the photoreduction of GO under laser irradiation. For individual QDs themselves, distinct photoblinking events with the decrease of fluorescence intensity can be observed. To further reveal the optical properties of QDs varied as a function of laser irradiation, the time-tagged, time-resolved and time-correlated single-photon counting (TTTR–TCSPC) technique was used to demonstrate the fluorescence intensity and lifetime simultaneously. Here, the irradiation durations under the control lasers of 0, 45, 90 and 135 s were selected for further studies. The duration of 0 s denotes the original monolayer GO, while the other durations denote RGO with different reduction degrees. To simplify, they are named RGO-1, 2, 3, respectively. For comparison, the QDs on glass were also studied.

Fluorescence intensity trajectories, photon counting histograms, and the corresponding time-resolved fluorescence decays for individual QDs on glass, GO and RGO-3 have been presented in Fig. 2b–d, respectively. It can be found that QDs under all three conditions feature the typical two-state, on–off blinking (Fig. 2b$_1$, c$_1$, and d$_1$, respectively) with clear separation, as the corresponding histograms shown in Fig. 2b$_2$, c$_2$, and d$_2$, respectively. Here, the on- and off-state refer to the state with high and low or non-fluorescence emission, respectively. The two states are separated by threshold fluorescence intensities, as the gray lines shown in Fig. 2b–d (the rule for the determination of threshold intensity can be found in Fig. S9†). One can find that the intensities of the on- and off-states under these conditions are significantly different. For QDs on glass, the intensities of the on- and off-states are 1315 and 82 cps, respectively. Thus, we can conclude that the fluorescence intensity of bare individual QDs on glass is 1233 cps. The time-resolved fluorescence decay for QDs on glass can be fitted by using the single exponential function,

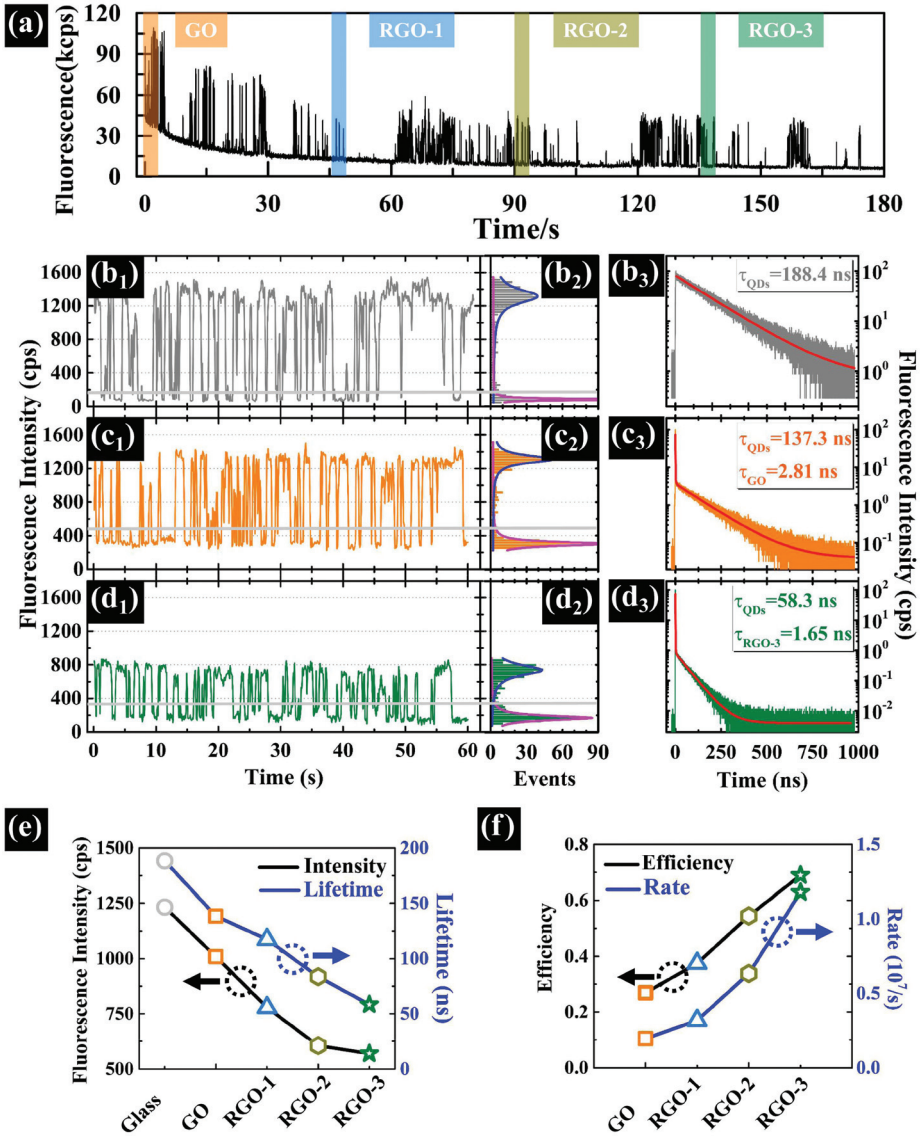

Fig. 2 (a) Fluorescence trajectory of CdSeTe/ZnS QDs on GO under the irradiation of a control laser. The laser power is 1 mW. (b–d) Fluorescence trajectories, photon counting histograms, and time-resolved fluorescence decays for individual CdSeTe/ZnS QDs on glass, GO, and RGO-3, respectively. The gray lines represent the thresholds separating the on- and off-states. (e) Fluorescence intensities and lifetimes for CdSeTe/ZnS QDs under five conditions. (f) The efficiencies and rates of the FRET process between CdSeTe/ZnS QDs and GO, and RGO-1, 2, 3, respectively.

$I(t) = I_0 + A\exp(t/\tau_{QDs/Glass})$, yielding the lifetime of QDs on glass, $\tau_{GO/Glass}$, to be 188.4 ns, as shown in Fig. 2b$_3$.

However, when the QDs are loaded on monolayer GO, the intensities of the on- and off-states are 1310 and 302 cps, respectively. The fluorescence intensity of 1008 cps for QDs on GO is lower than that on glass, suggesting the existence of interaction between QDs and GO. Furthermore, the intensity of the off-state for QDs on GO is much larger than that on glass, due to the fluorescence emission of GO itself. Note that the fluorescence background shows no significant change during TTTR–TCSPC measurements, totally different from the irradiation under the control laser (Fig. 2a). As we mentioned above, the negligible change in the fluorescence intensity can be attributed to the extremely weak reduction effect on GO under pulsed laser excitation. Unlike QDs on glass sharing a single long lifetime, the time-resolved fluorescence decay of QDs on GO displays a very short time decay and a long time decay. Two lifetimes have been determined by the double-exponential function, which are 2.81 ns and 137.3 ns, respectively. The short lifetime value can be attributed to the lifetime of GO fluorescence, consistent with previous reports.[32,33] Thus the value of 137.3 ns can be assigned as the lifetime of QDs, which is smaller than that on glass. The decrease in lifetime also suggests the interaction between QDs and GO. The interaction becomes stronger after GO irradiation under the control laser. This can be proved by the further decay in both the fluo-

Table 1 Fluorescence intensity, lifetime of QDs and GO, the efficiency and the rate of energy transfer from an individual QDs to GO, or RGO-1, 2, 3

	Substrate	Glass	GO	RGO-1	RGO-2	RGO-3
QDs	On-state (cps)	1315	1310	1035	798	735
	Off-state (cps)	82	302	257	194	166
	Intensity (cps)	1233	1088	778	604	569
	Lifetime (ns)	188.4	137.3	117.5	83.6	58.3
GO	Intensity (cps)		220	175	112	84
	Lifetime (ns)		2.81	2.04	1.73	1.65
FRET	Efficiency (%)		26.9	37.5	54.4	69.0
	Rate (10^7 s^{-1})		0.195	0.318	0.633	1.179

rescence intensity and lifetime of QDs on RGO-3, which are 569 cps and 58.3 ns, respectively, as presented in Fig. 2d. Further information about RGO-1 and RGO-2 can be found in Fig. S10.† The fluorescence intensity and lifetime of QDs under five conditions are also listed in Table 1.

Generally, the interactions in 0D–2D hybrid structures can be distinguished into two possibilities: FRET and charge transfer.[34,35] Both processes will result in the decay of fluorescence intensity and lifetime.[14] To explore that the interaction between QDs and GO originates from one of them or both processes, the dynamics of photoblinking events are analyzed. Photoblinking is usually associated with the charging of the core *via* intermittent tapping of the electrons or holes at the surface of the QDs and/or the surrounding film.[35] Thus, the charge transfer will substantially alter the dynamics of photoblinking. Cotlet's group has proved that the analysis on the probability distribution of photoblinking events (on- and off-state, respectively) can be used to discriminate the FRET and charge transfer between 0D and 2D hybrid materials,[14] such as QDs and GO used in this experiment.

The well-defined on- and off-states in fluorescence trajectories supply good conditions to build their probability distributions. The probability, $P(t)$, of an individual QD in the on- or off-state is defined as:[36]

$$P_i(t) = \frac{N_i(t)}{N_{i,\text{total}}} \times \frac{1}{\Delta t_{\text{avg}}} (i = \text{on or off}) \quad (1)$$

where $N_i(t)$ is the number of on- or off-states with the duration t, $N_{i,\text{total}}$ is the total number of on- or off-state events, and Δt_{avg} is the average of the time intervals to the preceding and following events. $P_{\text{on}}(t)$ and $P_{\text{off}}(t)$ for five conditions (on glass, GO and RGO-1, 2, 3, respectively) have been shown in Fig. 3, which present similar trends. Both $P_{\text{on}}(t)$ and $P_{\text{off}}(t)$ can be well fitted with a power law function, expressed as:[37]

$$P(t_i) = B_i \times t^{-\alpha_i} \ (i = \text{on or off}) \quad (2)$$

where α_i is the power law exponent and B_i is the amplitude. All the fitting parameters have been listed in Table 2.

Experimental investigations have indicated that the density of surface negative charge on RGO is much less than those on GO, due to the removal of oxygen-containing functional groups.[38,39] According to the previous reports,[40,41] if charge transfer dominates the interaction between QDs and GO, the power law exponent, α, of GO is expected to be smaller than that of RGO, due to less negative charge on RGO. Furthermore,

Table 2 Parameters of photoblinking events derived from the on- and off-state probabilities, from Fig. 3, for QDs deposited on glass, GO and RGO with different irradiation durations

	α_{on}	R^2	α_{off}	R^2
Glass	1.053	0.936	1.335	0.975
GO	0.949	0.977	1.259	0.994
RGO-1	0.962	0.978	1.347	0.989
RGO-2	0.919	0.955	1.355	0.967
RGO-3	0.949	0.939	1.207	0.967

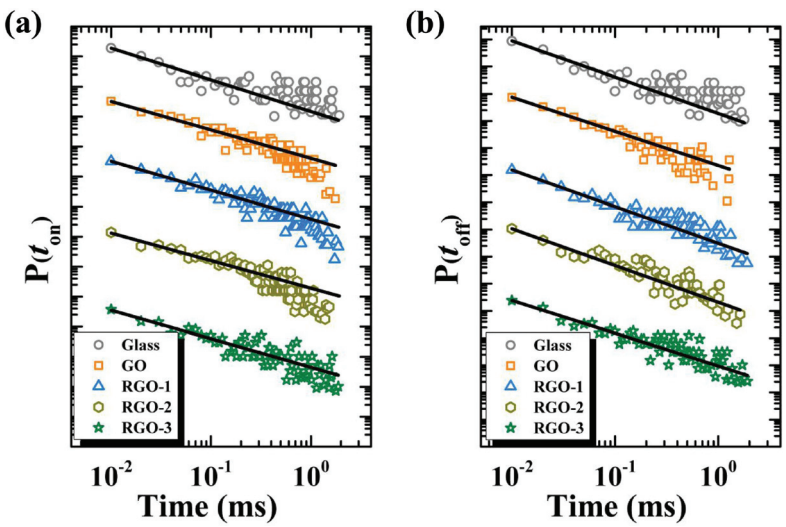

Fig. 3 Probability distributions of (a) $P_{\text{on}}(t)$ and (b) $P_{\text{off}}(t)$ for CdSeTe/ZnS QDs on glass (gray circle), GO (orange square), RGO-1 (blue triangle), RGO-2 (grass green hexagon), and RGO-3 (green pentacle), respectively. Solid lines are fits according to eqn (2).

by assuming non-interaction between QDs and glass, α for QDs on glass would be further smaller. However, the inconspicuous difference in the value of the power law exponents under five conditions, especially the lack of change from QDs on glass and on GO, strongly suggests that the charge transfer does not dominate the interaction.[14] Thus, we can conclude that FRET dominates the interaction and leads to the further decay of fluorescence intensity and lifetime, when the QDs are loaded on GO, as well as when the GO is converted to RGO by laser irradiation. An additional fact that supports our conclusion is that QDs and GO were separated by insulating the PMMA film with a thickness of 15 nm, which is much larger than the favorable distance for the occurrence of charge transfer.[42,43]

To quantitatively evaluate the FRET process from QDs to GO and RGO with different irradiation durations, the energy transfer efficiency, η_{FRET}, and the energy transfer rate, κ_{FRET}, can be derived from the lifetime of QDs under five conditions, according to the expressions:[14,27]

$$\eta_{FRET} = 1 - \frac{\tau_j}{\tau_{QDs/Glass}} \quad (3)$$

$$\kappa_{FRET} = \frac{1}{\tau_{FRET}} = \frac{1}{\tau_j} - \frac{1}{\tau_{QDs/Glass}} \quad (4)$$

where τ_j (j = QDs/GO or QDs/RGO) denotes the lifetime of QDs on GO or RGO, and $\tau_{QDs/Glass}$ denotes that on glass, regarded as the intrinsic lifetime of QDs. The derived parameters have been listed in Table 1. The efficiency of 69.0% for QDs on RGO-3 is much higher than that of 26.9% on GO, indicating the great increase in the interaction between QDs and GO. Meanwhile, the rate also improves from 0.195×10^7 s^{-1} to 1.179×10^7 s^{-1}. The change of the fluorescence intensity and lifetime of QDs as well as the modification of the efficiency and rate not only demonstrate the manipulation of the optical properties of the QDs, but also indicate the manipulation of the interaction between the QDs and surrounding environments. More importantly, this manipulation can be precisely controlled by altering the laser irradiation with the features of *in situ* manipulation, wireless steering and high spatial resolution.

To estimate the effect of anisotropic optical properties on this 0D–2D system and further prove the manipulation, the fluorescence lifetimes of more than 1000 individual QDs on glass or many monolayer GO films have been investigated. Fig. 4 presents the lifetime distributions of QDs under five conditions, and all these follow a normal distribution. The center value for QDs on glass is 168.4 ns, with the full width at half maximum (FWHM) to be 91.4 ns. Such a wide range mainly originates from the difference in the dot size and geometrical shape of the QDs, as shown in Fig. S2.† After the QDs are loaded on GO, the average lifetime decreases to 118.4 ns, suggesting that the substantial FRET has occurred between QDs and GO. The continuously decreased lifetime over the irradiation duration indicates that the interaction becomes stronger. Note that the FWHMs of the lifetimes of QDs on GO or RGO are close, but much narrower than those on glass, as listed in Table 3 and shown in Fig. 4f. The suppression of the anisotropy of the QDs may result from the FRET process; however, the underlying mechanism is still unclear. Furthermore, the fluorescence intensity histograms for these QDs under five conditions are presented in Fig. S11 and Table S1,† where the intensity of QDs on glass has been sub-

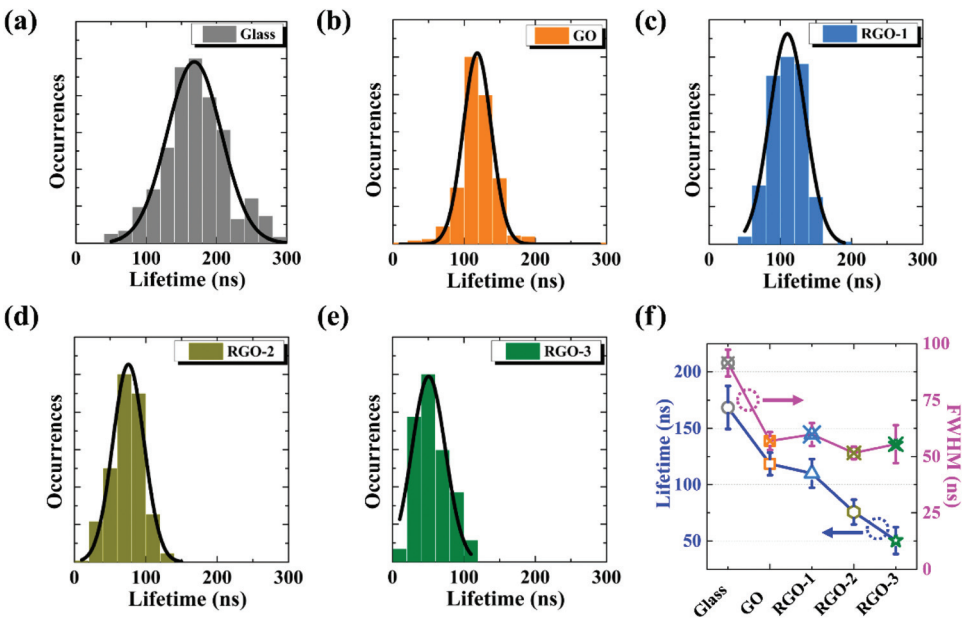

Fig. 4 Lifetime histograms for CdSeTe/ZnS QDs on (a) glass, (b) GO, (c) RGO-1, (d) RGO-2, and (e) RGO-3; (f) mean lifetime (blue line) and the full width at half-maximum (FWHM, pink line) for CdSeTe/ZnS QDs under the five conditions mentioned above, which were obtained from the Gauss fits of the histograms in panels a–e.

Table 3 The center values of fluorescence lifetime distributions and the FWHM of QDs on glass, GO and RGO with different irradiation durations, and the corresponding energy transfer efficiency and rate

	Lifetime (ns)	FWHM (ns)	η_{FRET} (%)	κ_{FRET} (10^7 s^{-1})
Glass	168.4	91.4		
GO	118.4	56.9	29.7	0.251
RGO-1	110.0	59.8	34.7	0.315
RGO-2	75.7	51.6	55.0	0.727
RGO-3	50.5	55.5	70.0	1.386

stantially decreased from 1290 cps to 578 cps compared to that on RGO-3.

The center values and FWHMs of QDs under five conditions have been listed in Table 3. According to the statistical analyses, the energy transfer efficiency and rate for this 0D–2D system can be determined by using eqn (1) and (2) as well. The calculated results are listed in Table 3 and shown in Fig. 5, which are similar to that of individual QDs, as shown in Fig. 2e. The efficiency is enhanced from 29.7% to 70.0%, and the rate is increased from 0.251×10^7 s^{-1} to 1.386×10^7 s^{-1}. The rate of FRET as a function of laser irradiation can be well explored based on the classical Förster theory,[22] where the rate is proportional to the overlap integral of donor's fluorescence spectrum, $F_D(\lambda)$, and acceptor's absorption spectrum, $\varepsilon_A(\lambda)$. The equation can be expressed as:

$$\kappa_{FRET} \propto \int_0^\infty F_D(\lambda)\varepsilon_A(\lambda)\lambda^4 d\lambda \quad (5)$$

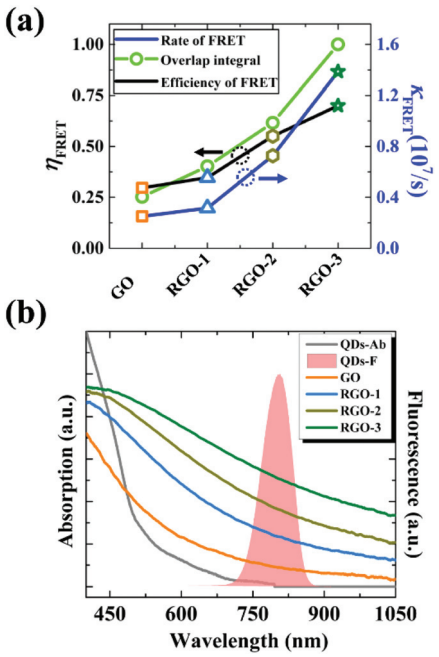

Fig. 5 (a) Derived efficiencies and rates of the FRET process, as well as the calculated overlap integral between QDs and GO or RGO-1, 2, 3, respectively. (b) Absorption and fluorescence spectra of CdSeTe/ZnS QDs, and the absorption spectra of GO, and RGO-1, 2, 3, respectively.

In this experiment, QDs act as the donor and GO or RGO acts as the acceptor. Thus the $F_D(\lambda)$ is the fluorescence emission spectrum of QDs, and $\varepsilon_A(\lambda)$ is the absorption spectrum of GO or RGO with different irradiation durations. The normalized fluorescence spectrum of QDs and absorption spectra of GO and RGO have been presented in Fig. 5b. Note that with the increase in irradiation duration, the absorption of RGO becomes stronger. This phenomenon is consistent with previous studies,[39,44] where the increased absorption can be attributed to the restoration of electronic conjugation with an increased reduction degree. The calculated energy transfer rate for QDs on GO and RGO, as circles shown in Fig. 5a, agrees well with the experimental results.

The statistical results further prove that the optical properties of QDs and the interaction between QDs and GO can be manipulated by varying the absorption spectra of GO through laser irradiation. This approach has many outstanding features. Firstly, this process can be performed at any stage of QD-based device fabrication, especially providing an *in situ* manipulation after device fabrication, according to the demand in practical applications. Next, the control laser is focused by a high numerical aperture with the laser spot close to the diffraction limit, therefore the manipulation has high spatial resolution naturally. This allows the users to manipulate the optical properties and interactions of QDs in any desired areas, rather than the full device. Thirdly, the manipulation is achieved by varying the duration of laser irradiation, which can be operated remotely and flexibly. The manipulation can also be performed in other ways, such as by changing the power,[31] wavelength,[45] and repetition of the control laser.[46] Furthermore, this method enables the all-optical manipulation in non-contact form, thus the micro-electrodes and other treatments (such as electrochemical etching) are not required here, which will increase the complexity and difficulty of the manipulation, and may damage QDs. These outstanding features, especially *in situ* manipulation with high spatial resolution, make QDs potential for lifetime-and-intensity multiplexing,[47] which will provide an enhanced information capacity in QD-based optical recording, encryption and data storage.[48,49] In addition, by manipulating the FRET process, the optical properties of the donor (QDs) have been successfully modified in this work. This result also inspires us to control the optical properties of the acceptor by the FRET process.[50]

3. Conclusion

In summary, we propose a scheme to manipulate the efficiency and rate of the FRET process between QDs and monolayer GO, by varying the absorption spectrum of GO through laser irradiation, thus to realize the modification on the optical properties of QDs. The mean fluorescence intensity of QDs has been substantially decreased from 1290 cps on PMMA to 578 cps on RGO, and the corresponding fluorescence lifetime has been reduced from 168.4 ns to 50.5 ns. This

scheme provides a new approach for tuning the properties of donors (QDs here) in such 0D–2D hybrid structures by changing the optical properties of the acceptor (GO). The degree of manipulation can be controlled flexibly by controlling the duration, power density, wavelength and repetition of the irradiated laser. Our scheme, with the features of *in situ* manipulation, high spatial resolution and wireless steering, is significant for the tuning of the properties of optoelectronic devices based on QDs from the viewpoints of both fundamental and practical applications.

4. Methods

4.1 Sample preparation

GO was synthesized by the modified Hummers method, and the detailed description can be found in our previous studies.[31] PMMA (MW = 15 000, T_g = 82 °C, dielectric constant 3.4) was purchased from Aldrich and without further treatment. The NIR CdSeTe/ZnS core–shell QDs (Qdot® 800 ITK TM Organic Quantum Dots) were ordered from Thermo Fisher Scientific. The GO film was prepared by spin-coating the GO dispersion with a concentration of 1 mg mL^{-1} on a cleaned glass coverslip. The parameters of spin-coating were set as 500 rmp for 12 s firstly, and then 3000 rmp for 60 s. The as-prepared GO film was dried at room temperature under a nitrogen atmosphere for 10 hours to remove the remaining solvent. According to the AFM characterization, as shown in Fig. 1b, the monolayer GO film has been fabricated successfully on the glass coverslip. To control the interaction between GO and QDs, the PMMA film was then deposited on monolayer GO by the spin-coating method as well. The operation parameters of spin-coating were 500 rmp for 5 s, 3000 rmp for 60 s, and 600 rmp for 10 s in turns to ensure the thickness of 15 nm. Furthermore, the manipulation of FRET with other thicknesses has also been investigated to determine the optimum conditions, as in Fig. S12.† The prepared PMMA film was dried under a nitrogen atmosphere. Lastly, QDs with a concentration of ~10^{-9} mol L^{-1} were spin-coated on the top of the PMMA film at 3000 rmp for 20 s. AFM characterization of bare QDs on the glass coverslip as well as the TEM image, as presented in Fig. S2,† show that the size of QDs is in the region of 3.6–9.6 nm.

4.2 Optical setup

To control the reduction degree of GO and probe the optical properties of each individual QD, a home-built scanning confocal system based on an inverted microscope (Nikon, TE2000-U) was used to irradiate GO and measure the fluorescence of QDs. The detailed descriptions of this optical setup can be found in our previous studies.[32,51] Particularly, a 485 nm laser with both CW and pulsed wave modes was used here. The laser beam was tightly focused by a 100× oil immersion objective lens with a high numerical aperture (NA = 1.3). The focused laser spot was about 300 nm in diameter, mainly limited by diffraction. The sample was placed on the piezoelectric translation nano-stage (PZT, Tritor, 200/20SG). Fluorescence imaging of GO and QDs was created by moving the sample with respect to the focused laser beam in a programmable and control way. The step size of the nano-stage was 180 nm, and the speed was kept constant at 18 μm s^{-1}. The fluorescence from GO and QDs was collected by using the same objective. After passing through a dichroic mirror (Semrock, Di01-R488-25 × 36), and a long-pass filter (Semrock, BLP01-496R-25) to block the back scattered laser as well as the background signal, the fluorescence was further filtered spatially using a 100 μm pinhole and detected by using a single photon detector (PerkinElmer, SPCM-AQR-15). The synchronization of the pulsed laser and the outputs of the detectors were fed into a TTTR–TCSPC data acquisition card (DAC, HydraHarp 400, PicoQuant), by which the time-dependence information for all of the detected photons can be recorded simultaneously. Consequently, the fluorescence intensity and lifetime can be obtained simultaneously. The time resolution of the system is approximately 150 ps.

Conflicts of interest

There are no conflicts to declare.

Acknowledgements

This project is sponsored by the National Key Research and Development Program of China (Grant No. 2017YFA0304203), the National Natural Science Foundation of China (Grant No. 11434007), the Natural Science Foundation of China (No. 61875109, 61527824, U1510133, 61675119, 11504216, and 61605104), PCSIRT (No. IRT_17R70), 1331KSC and 111 project (Grant No. D18001).

Notes and references

1 J. Zhou, Y. Yang and C. Y. Zhang, *Chem. Rev.*, 2015, **115**, 11669–11717.
2 H. Zhong, Z. Bai and B. Zou, *J. Phys. Chem. Lett.*, 2012, **3**, 3167–3175.
3 Y. Shirasaki, G. J. Supran, M. G. Bawendi and V. Bulović, *Nat. Photonics*, 2013, **7**, 13–23.
4 G. H. Carey, A. L. Abdelhady, Z. Ning, S. M. Thon, O. M. Bakr and E. H. Sargent, *Chem. Rev.*, 2015, **115**, 12732–12763.
5 G. Konstantatos, I. Howard, A. Fischer, S. Hoogland, J. Clifford, E. Klem, L. Levina and E. H. Sargent, *Nature*, 2006, **442**, 180–183.
6 F. Hetsch, N. Zhao, S. V. Kershaw and A. L. Rogach, *Mater. Today*, 2013, **16**, 312–325.
7 J. Claudon, J. Bleuse, N. S. Malik, M. Bazin, P. Jaffrennou, N. Gregersen, C. Sauvan, P. Lalanne and J. M. Gerard, *Nat. Photonics*, 2010, **4**, 174–177.

8 B. S. Mashford, M. Stevenson, Z. Popovic, C. Hamilton, Z. Zhou, C. Breen, J. Steckel, V. Bulovic, M. Bawendi, S. Coe-Sullivan and P. T. Kazlas, *Nat. Photonics*, 2013, **7**, 407–412.
9 I. Moreels, K. Lambert, D. Smeets, D. De Muynck, T. Nollet, J. C. Martins, F. Vanhaecke, A. Vantomme, C. Delerue, G. Allan and Z. Hens, *ACS Nano*, 2009, **3**, 3023–3030.
10 X. G. Peng, *Adv. Mater.*, 2003, **15**, 459–463.
11 R. Buonsanti and D. J. Milliron, *Chem. Mater.*, 2013, **25**, 1305–1317.
12 M. D. Regulacio and M. Y. Han, *Acc. Chem. Res.*, 2010, **43**, 621–630.
13 H. M. Zhu, N. H. Song and T. Q. Lian, *J. Am. Chem. Soc.*, 2010, **132**, 15038–15045.
14 H. Zang, P. K. Routh, Y. Huang, J. S. Chen, E. Sutter, P. Sutter and M. Cotlet, *ACS Nano*, 2016, **10**, 4790–4796.
15 Y. Yu, Z. H. Ji, S. Zu, B. W. Du, Y. M. Kang, Z. W. Li, Z. K. Zhou, K. B. Shi and Z. Y. Fang, *Adv. Funct. Mater.*, 2016, **26**, 6394–6401.
16 F. Prins, A. J. Goodman and W. A. Tisdale, *Nano Lett.*, 2014, **14**, 6087–6091.
17 S. H. Zhao, Y. Lv and X. J. Yang, *Nanoscale Res. Lett.*, 2011, **6**, 6.
18 Q. H. Wang, K. Kalantar-Zadeh, A. Kis, J. N. Coleman and M. S. Strano, *Nat. Nanotechnol.*, 2012, **7**, 699–712.
19 Z. Y. Chen, S. Berciaud, C. Nuckolls, T. F. Heinz and L. E. Brus, *ACS Nano*, 2010, **4**, 2964–2968.
20 A. Raja, A. Montoya Castillo, J. Zultak, X. X. Zhang, Z. Ye, C. Roquelet, D. A. Chenet, A. M. van der Zande, P. Huang, S. Jockusch, J. Hone, D. R. Reichman, L. E. Brus and T. F. Heinz, *Nano Lett.*, 2016, **16**, 2328–2333.
21 K. M. Goodfellow, C. Chakraborty, K. Sowers, P. Waduge, M. Wanunu, T. Krauss, K. Driscoll and A. N. Vamivakas, *Appl. Phys. Lett.*, 2016, **108**, 021101.
22 J. R. Lakowicz, *Principles of fluorescence spectroscopy*, Kluwer Academic/Plenum, New York, 2nd edn, 1999, pp. 443–446.
23 Z. X. Pan, K. Zhao, J. Wang, H. Zhang, Y. Y. Feng and X. H. Zhong, *ACS Nano*, 2013, **7**, 5215–5222.
24 A. Zintchenko, A. S. Susha, M. Concia, J. Feldmann, E. Wagner, A. L. Rogach and M. Ogris, *Mol. Ther.*, 2009, **17**, 1849–1856.
25 M. Li, X. Zhou, S. Guo and N. Wu, *Biosens. Bioelectron.*, 2013, **43**, 69–74.
26 Y. Gao, C. Qin, Z. Qiao, B. Wang, W. Li, G. Zhang, R. Chen, L. Xiao and S. Jia, *Carbon*, 2015, **93**, 843–850.
27 S. Sampat, T. Guo, K. Zhang, J. A. Robinson, Y. Ghosh, K. P. Acharya, H. Htoon, J. A. Hollingsworth, Y. N. Gartstein and A. V. Malko, *ACS Photonics*, 2016, **3**, 708–715.
28 H. F. Dong, W. C. Gao, F. Yan, H. X. Ji and H. X. Ju, *Anal. Chem.*, 2010, **82**, 5511–5517.
29 Z. M. Zhou, J. Zhou, J. Chen, R. N. Yu, M. Z. Zhang, J. T. Song and Y. D. Zhao, *Biosens. Bioelectron.*, 2014, **59**, 397–403.
30 R. Wu, R. Chen, Y. Gao, G. Zhang, L. Xiao and S. Jia, *Jpn. J. Appl. Phys.*, 2013, **52**, 125501.
31 Z. Qiao, C. Qin, W. He, Y. Gong, G. Zhang, R. Chen, Y. Gao, L. Xiao and S. Jia, *Opt. Express*, 2017, **25**, 31025–31035.
32 W. He, C. Qin, Z. Qiao, G. Zhang, L. Xiao and S. Jia, *Carbon*, 2016, **109**, 264–268.
33 J. Shang, L. Ma, J. Li, W. Ai, T. Yu and G. G. Gurzadyan, *Sci. Rep.*, 2012, **2**, 792.
34 S. Roy, G. P. Neupane, K. P. Dhakal, J. Lee, S. J. Yun, G. H. Han and J. Kim, *J. Phys. Chem. C*, 2017, **121**, 1997–2004.
35 E. Shafran, B. D. Mangum and J. M. Gerton, *Nano Lett.*, 2010, **10**, 4049–4054.
36 S. Y. Jin and T. Q. Lian, *Nano Lett.*, 2009, **9**, 2448–2454.
37 F. Cichos, C. Vonborczyskowski and M. Orrit, *Curr. Opin. Colloid Interface Sci.*, 2007, **12**, 272–284.
38 M. J. Li, C. M. Liu, H. B. Cao and Y. Zhang, *Adv. Mater. Res.*, 2013, **716**, 127–131.
39 M.-J. Li, C.-M. Liu, Y.-B. Xie, H.-B. Cao, H. Zhao and Y. Zhang, *Carbon*, 2014, **66**, 302–311.
40 H. Yuan, E. Debroye, G. Caliandro, K. P. Janssen, J. van Loon, C. E. Kirschhock, J. A. Martens, J. Hofkens and M. B. Roeffaers, *ACS Omega*, 2016, **1**, 148–159.
41 B. Li, G. Zhang, Z. Wang, Z. Li, R. Chen, C. Qin, Y. Gao, L. Xiao and S. Jia, *Sci. Rep.*, 2016, **6**, 32662.
42 A. Paul, R. M. Watson, E. Wierzbinski, K. L. Davis, A. Sha, C. Achim and D. H. Waldeck, *J. Phys. Chem. B*, 2010, **114**, 14140–14148.
43 X. Ji, W. Wang and H. Mattoussi, *Phys. Chem. Chem. Phys.*, 2015, **17**, 10108–10117.
44 S. Bhattachraya, R. Maiti, A. C. Das, S. Saha, S. Mondal, S. K. Ray, S. N. B. Bhaktha and P. K. Datta, *J. Appl. Phys.*, 2016, **120**, 013101.
45 Y. C. Li, T. F. Yeh, H. C. Huang, H. Y. Chang, C. Y. Lin, L. C. Cheng, C. Y. Chang, H. Teng and S. J. Chen, *Opt. Express*, 2014, **22**, 19726–19734.
46 E. Kymakis, C. Petridis, T. D. Anthopoulos and E. Stratakis, *IEEE J. Sel. Top. Quantum Electron.*, 2014, **20**, 106–115.
47 M. Y. Han, X. H. Gao, J. Z. Su and S. Nie, *Nat. Biotechnol.*, 2001, **19**, 631–635.
48 B. Senyuk, N. Behabtu, A. Martinez, T. Lee, D. E. Tsentalovich, G. Ceriotti, J. M. Tour, M. Pasquali and I. I. Smalyukh, *Nat. Commun.*, 2015, **6**, 7157.
49 P. Zijlstra, J. W. Chon and M. Gu, *Nature*, 2009, **459**, 410–413.
50 Z. W. Li, R. Q. Ye, R. Feng, Y. M. Kang, X. Zhu, J. M. Tour and Z. Y. Fang, *Adv. Mater.*, 2015, **27**, 5235–5240.
51 H. T. Zhou, C. B. Qin, R. Y. Chen, G. F. Zhang, L. T. Xiao and S. T. Jia, *Appl. Phys. Lett.*, 2014, **105**, 5.

